Supporting information for

Reversible Excited State Electron Transfer in an Acceptor-Acceptor Hetero Dyad

Table of Contents:

Experimental:

Synthetic Methods and Materials. All chemicals and solvents were purchased from commercial suppliers and used as received except for the mono-brominated PDI (Br-PDI) that was synthesized according to literature procedures.[1] The Phenol-ADOTA and ADOTA-Ref were synthesized according to literature procedures.[2] The synthesis of both PDI-ADOTA and PDI-OPh was based on the reported synthesis of inserting two phenol groups by Lin, M-J. et al.[3]

Mass spectra were recorded on an ESP-MALDI-FT-ICR instrument equipped with a 7 T magnet (the instrument was calibrated using sodium trifluoroacetate cluster ions prior to acquiring the spectra). 1H and 13C NMR spectra were acquired on a Bruker 500 MHz instrument equipped with a (noninverse) cryoprobe. All chemical shift values in both ^{1}H and ^{13}C NMR spectra are referenced to the residual solvent peak ($CDCl^3$ δ H = 7.26, δ C = 77.16).

Spectroscopic methods. All spectroscopy was recorded in 1 cm path length UV Quartz cuvettes. The UV–vis absorption spectra were recorded either on a Cary 300 UV–vis double beam spectrophotometer (Agilent Technologies, Santa Clara, USA) or a Lambda1050 UV/Vis/NIR double beam spectrophotometer (PerkinElmer, Massachusetts, USA) using the pure solvent as the baseline.

Fluorescence spectra and lifetimes were measured using a FluoroTime 300 (PicoQuant, Berlin, Germany) system with a hybrid PMT detector. The fluorescence emission spectra were recorded using a xenon lamp as the excitation source, and all spectra were corrected for the wavelength-dependent sensitivity of the detector. For all fluorescence measurement the absorption was held below 0.1 at the excitation wavelength.

The fluorescence quantum yields of the compounds were measured relative to pr-ADOTA which has a well-established quantum yield of 83 % in DCM.[4]

For the fluorescence lifetimes, the decays were measured by time-correlated single photon counting (TCSPC). Samples were excited using a pulsed solid-state 530 nm laser (LDH-D-TA-530B), and the emission monochromator was set to 600 nm for all fluorophores. Decays were analyzed using the FluoFit software package (PicoQuant), where the decay ($I_f(t)$) was fitted by iterative reconvolution with a sum of exponentials:

$$I_f(t) = \sum a_i \exp\left(-\frac{t}{\tau_i}\right)$$

In this equation, a_i is the amplitude, and τ_i is the fluorescence lifetime of the I'th component. The instrument response function (IRF) was recorded using a scattering suspension of Ludox with the emission monochromator set to the excitation wavelength. The angle between the excitation and emission polarizers for all fluorescence measurements was set to magic angle (54.7°).

Absorption measurements with 0–3 eq. $CoCp_2$ with THF and DMF as solvents were performed inside an oxygen-free glovebox. Reduction of PDI-ADOTA in DCM was unsuccessful due to rapid oxidation of the reduced molecule.

Femtosecond (fs) Transient absorption experiments were performed by using a femtosecond pump–probe setup. Laser pulses (796 nm, 60 fs pulse length, 4 kHz repetition rate) were generated using a regenerative amplifier (Solstice Ace) seeded by a femtosecond oscillator (Mai Tai SP, both Spectra Physics). The pulsed laser light was divided into two parts to use for pump and probe beams. For the pump, we used the TOPAS C (Light Conversion) to obtain pump light with a central wavelength located at 535 nm. The pump light energy was set to 0.3 μJ. The spot size was approximately 0.2 mm^2. For the probe, we used supercontinuum white light generated from a thin CaF_2 plate, the spot size was approximately 0.05 mm^2 for probe. The mutual polarization between the pump and probe beams was set to the magic angle (54.7°) by placing a Berek compensator in the pump beam. To avoid photo-damage, the sample was moved to a fresh spot after each time delay point. There was no photodegradation after fs-TA experiments by checking the steady-state absorption spectra. The global analysis was performed by Glotaran software package (http://glotaran.org).

For the global analysis, our strategy is the standard framework of singular-value decomposition (SVD) followed by a sum-of-exponential-decays model fit to the data. This corresponds to using a set of coupled first-order differential equations to treat the photo-excited dyad. Considering the relaxing process of the photo-excited dyad, we used a sequential and unidirectional relaxation model, in which three excited-states with one-way state-to-state transfer are considered. Based on the global analysiss.[5], we get these spectra from the minimally complex representation of multi-exponential decays: the *evolution-associated spectra* (EAS, as shown in Figure S16)[6] and the corresponding lifetimes (Table S4).

Electrochemical Methods. Cyclic voltammetry (CV) was carried out at room temperature in DCM and DMF containing Bu_4NPF_6 (0.1 M) as the supporting electrolyte using a CHI series 600C instrument driven by CHI600C Electrochemical Analyzer software for DCM data and ECi-100-potentiostat for the DMF measurements. The working electrode was a circular glassy carbon disk (d = 3 mm), the counter electrode was a platinum wire, and the reference electrode was a silver wire immersed in the mixture and physically separated from the solution containing the substrate by a ceramic frit. The potential of the reference electrode was determined vs the ferrocene/ferrocenium (Fc/Fc^+) redox couple in separate experiments, once before and once after all samples were measured. The CV voltage scan rates were 0.05, 0.10, 0.15, and 0.20 V/s for reduction measurements except for in DMF were the scan rates was 0.05 and 0.10 V/s. *iR* compensation was used in all measurements. Solutions were purged with N_2 for at least 10 minutes before measuring, while a steady flow of N_2 above the solution was maintained during the measurement. The formal potentials for the reversible one electron reduction was determined by CV.

Synthesis

PDI-ADOTA – (Dyad)

To a RBF Br-PDI (89 mg, 0.11 mmol), Phenol-ADOTA (91 mg, 0.18 mmol), oven dried K_2CO_3 (47 mg, 0.34 mmol), and a stirring bar were added. The RBF was sealed with a septum, flushed with N_2 gas, and evacuated and refilled with N_2 gas 2 times. Anhydrous NMP (3.5 mL) was added as the solvent. The mixture was stirred at 90 °C in an oil bath. After 2.5 h the mixture was left to cool down, once ambient temperature was reached the mixture was added to 0.2 M KPF_6 (200 mL) which was acidified with 1 M HCl (10 mL). The formed precipitate was isolated by vacuum filtration washed off the filter using DCM and concentrated in vacuo. The crude product was purified by column chromatography (SiO_2) multiple times, first with a gradient of EtOAC (0 → 5 %) and 1 % MeOH in DCM and then EtOAc (0 – 5 %) in DCM twice. The pure product was isolated and concentrated in vacuo. Yield: 56 mg, 40 %.

^{1}H NMR (400 MHz, $CDCl_3$) δ 9.50 (d, *J* = 8.3 Hz, 1H), 8.80 – 8.69 (m, 5H), 8.50 (s, 1H), 8.11 (t, *J* = 8.5 Hz, 2H), 8.05 (t, *J* = 8.5 Hz, 1H), 7.71 – 7.64 (m, 2H), 7.55 – 7.44 (m, 6H), 6.98 (d, *J* = 8.7 Hz, 2H), 5.25 – 5.14 (m, 2H), 2.30 – 2.20 (m, 4H), 1.94 – 1.82 (m, 4H), 1.39 – 1.19 (m, 24H), 0.88 – 0.79 (m, 12H).

^{13}C NMR (126 MHz, $CDCl_3$) δ 164.73, 163.42, 157.45, 153.76, 153.24, 152.84, 142.31, 142.13, 140.62, 139.81, 134.87, 134.32, 133.17, 132.73, 131.02, 129.47, 128.91, 128.84, 127.16, 127.02, 125.74, 124.05, 123.06, 121.35, 112.03, 111.41, 109.98, 108.83, 106.08, 54.91, 32.47, 31.90, 31.87, 29.85, 26.79, 26.77, 22.71, 22.69, 13.67.

HR-MS (MALDI-TOF) m/z: [M^+] Calcd for $C_{96}H_{78}N_4O_{10}^+$, 1446.57180; found, 1446.59705.

PDI-OPh

To a dry RBF equipped with a stirring bar, Br-PDI (64 mg, 0.08 mmol), phenol (30 mg, 0.32 mmol), and oven dried K_2CO_3 (42 mg, 0.30 mmol) were added. The flask was sealed with a septum, evacuated and refilled with argon three times in total. Anhydrous NMP (5 mL) was added and the reaction was left stirring at 90 °C in an oil bath. After 6 h, heating was removed and the reaction mixture was added to 50 mL of H_2O, and extracted with EtOAc (8 × 25 mL). The organic phase was dried with Na_2SO_4, filtered, and concentrated in vacuo. The solid material was purified by column chromatography twice (SiO_2), first in 1:1 hexanes/EtOAc and then 1:1 hexanes/DCM to yield the pure product. Yield: 49 mg, 62 %.

^{1}H NMR (500 MHz, CD_2Cl_2) δ 9.58 (s, 1H), 8.73 (d, *J* = 8.1 Hz, 1H), 8.69 (s, 2H), 8.62 (s, 2H), 8.21 (s, 1H), 7.50 (t, *J* = 8.0 Hz, 2H), 7.31 (t, *J* = 7.5 Hz, 1H), 7.22 (d, *J* = 7.6 Hz, 2H), 5.20 – 5.12 (m, 2H), 2.37 – 2.11 (m, 4H), 1.87 – 1.77 (m, 4H), 1.39 – 1.13 (m, 24H), 0.91 – 0.75 (m, 12H).

^{13}C NMR (126 MHz, $CDCl_3$) δ 164.10, 156.34, 154.95, 134.57, 133.88, 130.80, 130.56, 129.45, 128.81, 128.72, 127.19, 126.07, 125.48, 124.43, 123.76, 122.54, 119.90, 54.80, 32.46, 32.44, 31.89, 31.85, 29.85, 26.76, 26.75, 22.70, 22.68, 14.18, 14.17.

HR-MS (MALDI-TOF) m/z: [M+$^+$] Calcd for $C_{52}H_{58}N_2O_5^+$, 790.43457; found, 790.43208.

Spectroscopy:

Table S1. Overview of optical properties and HOMO and LUMO energies in DCM.

	ADOTA-Ref	PDI-OPh	PDI-ADOTA (PDI unit)	PDI-ADOTA sh (ADOTA unit)
λ_{abs} (nm)	548	530	523	545
λ_{emi} (nm)	568	555		559
ε (M^{-1} cm^{-1})	14900	46000	62900	22700
τ (ns)[a]	19.4	4.6		11.2
Φ_f (%)[b]	73	86		31
$k_f \times 10^6$ (s^{-1})[c]	38	186		28
$k_{nr} \times 10^6$ (s^{-1})[d]	14	31		62
E_{00} (eV)[e]	2.22	2.29	2.31[f]	2.24
Stokes shift (cm^{-1})	643	850		426
$E^{0'}$ red (LUMO) (V vs Fc/Fc^+)[g]	–0.98	–1.12	–1.16	–1.01
HOMO energy[h]	1.24	1.17	1.16	1.23

[a]Intensity weighted average fluorescence lifetime. [b]Measured using pr-ADOTA as the reference (Φ_f = 83 %)[4]. [c]$k_f = \Phi_f / \tau$. [d]$k_{nr} = (1/\tau) - k_f$. [e]Energy of the $S_0 \rightarrow S_1$ (E_{00}) found as the average of λ_{abs} and λ_{emi} in cm^{-1} then multiplied with 0.00012398 to go from cm^{-1} to eV. [f]Calculted by addition of ½Stokes shift from PDI-OPh added to λ_{abs} in cm^{-1} and then converting to eV. [g]From electrochemistry. [h]HOMO energy (relative to Fc/Fc^+) found as the sum of reduction potential and E_{00}

Table S2. Fluorescence lifetimes in solvent mixtures of DCM with different v% ACN. Fluorescence decays and fits are shown in Figures S17–24.

	Solvent	τ_1 (ns)	Frac. Int. (%)	τ_2 (ns)	Frac. Int. (%)	τ_3 (ns)	Frac. Int. (%)	τ_{av} (ns)[a]	QY (%)[b]
ADOTA-Ref	0 v% ACN	19.4	100	-	-	-	-	-	73
	50 v% ACN	19.0	100	-	-	-	-	-	71
PDI-OPh	0 v% ACN	4.6	100	-	-	-	-	-	86
	50 v% ACN	4.6	100	-	-	-	-	-	82
PDI-ADOTA	0 v% ACN	11.4	97	0.2	1	5.1	2	11.2	31
	10 v% ACN	3.5	66	0.2	6	5.1*	28	3.7	8.8
	25 v% ACN	1.3	68	0.2	17	5.1	15	1.7	4.1
	50 v% ACN	0.7	80	0.1	12	5.2	8	1.0	3.1

*Locked at 5.1 ns during fitting, since τ_1 and τ_3 in this solvent mixture are so close that resolving them is not possible, this is also likely why the fractional intensity is so high for τ_3 as an artefact of the fitting. [a]Intensity weighted average. [b]Calculated from max peak in DCM.

Based on the transient absorption data we would expect only two components in the fluorescence lifetime for PDI-ADOTA. However, we observe a third component (τ_3), which is very low in intensity (Fractional intensity of 2%). There are several possible explanations to this. The most logic explanation is that there is a minute impurity (below 1 %) which is highly fluorescent. Normally even small amounts of impurity are detectable in absorption, emission and excitation spectra but in this case, it was not observed hence the quantity of said impurity must be low. Another possible explanation is that the dyad has a conformation which has a FLT of 5 ns, we have probed in order to see if this was a conformational "impurity" by doing spectra at elevated temperatures, but that did not result in any significant changes in this component. Anyhow the low intensity of τ_3 allows us to explain and characterize the properties and excited state processes of and in PDI-ADOTA.

Table S3. Rate constants in solvent mixtures of DCM with different v% ACN.

	Solvent	τ_{av} (ns)[a]	QY (%)[b]	k_f (10^6 s^{-1})	k_{nr} (10^6 s^{-1})
ADOTA-Ref	0 v% ACN	19.4	73	38	14
	50 v% CAN	19.0	71	38	15
PDI-OPh	0 v% ACN	4.6	86	186	31
	50 v% ACN	4.6	82	178	40
PDI-ADOTA	0 v% ACN	11.2	31	28	62
	10 v% ACN	3.7	8.8	24	246
	25 v% ACN	1.7	4.1	24	564
	50 v% ACN	1.0	3.1	31	969

[a]Intensity weighted average fluorescence lifetime. [b]Measured using pr-ADOTA as the reference (Φ_f = 83 %)[4]. [c]$k_f = \Phi_f / \tau$. [d]$k_{nr} = (1/\tau) - k_f$.

Steady-state spectroscopy

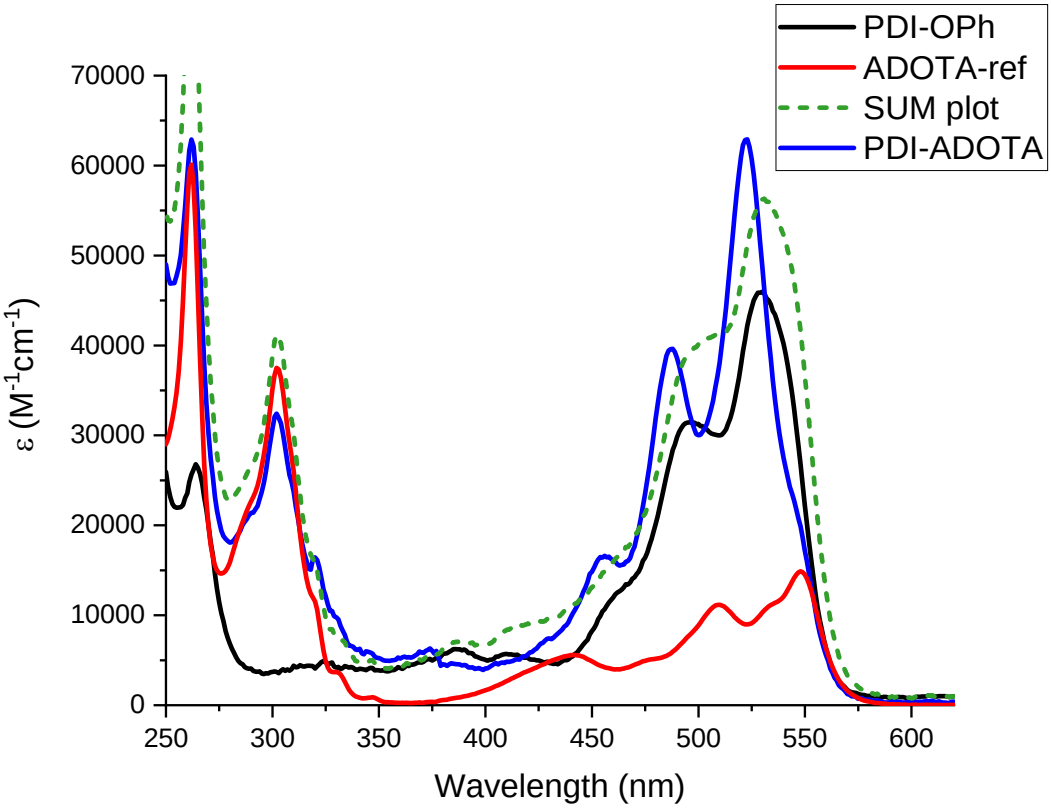

Figure S1. Molar absorptions coefficient plot in DCM, including a sum-plot of PDI-OPh and ADOTA-Ref compounds.

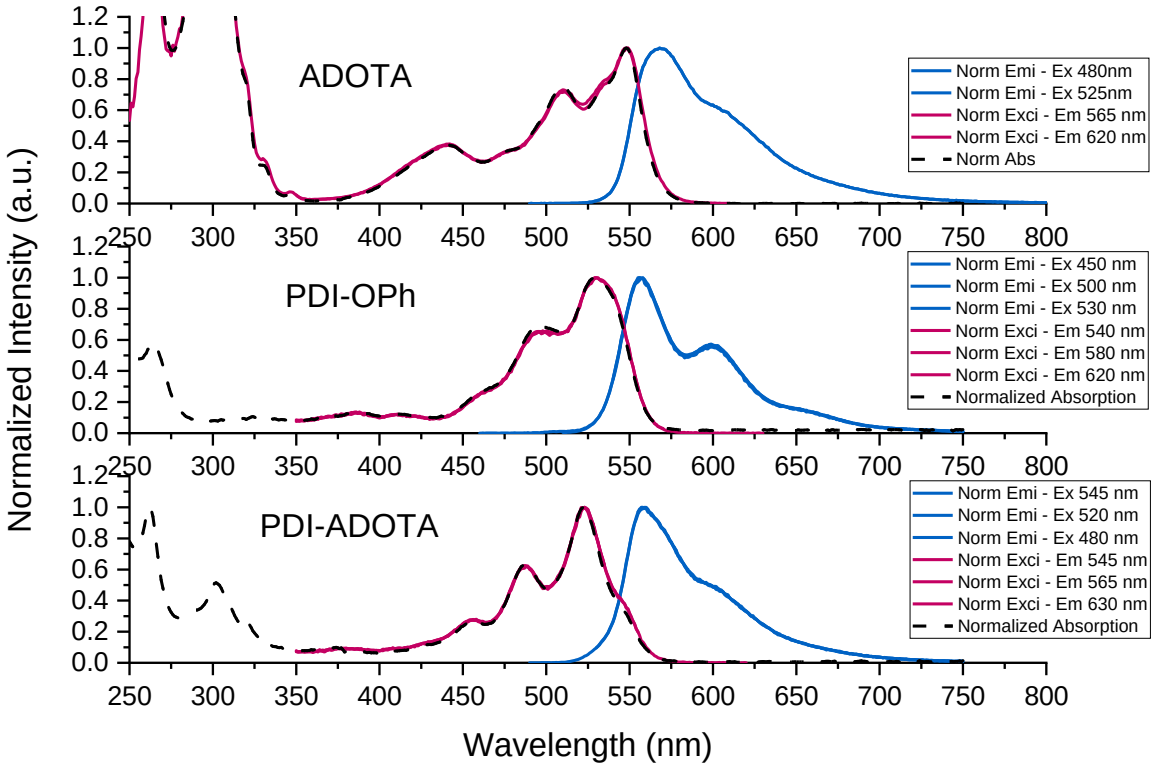

Figure S2. Normalized absorption, excitation and emission spectra in DCM, with excitation spectra obtained at 3 different wavelengths and emission spectra from 3 different excitation wavelengths

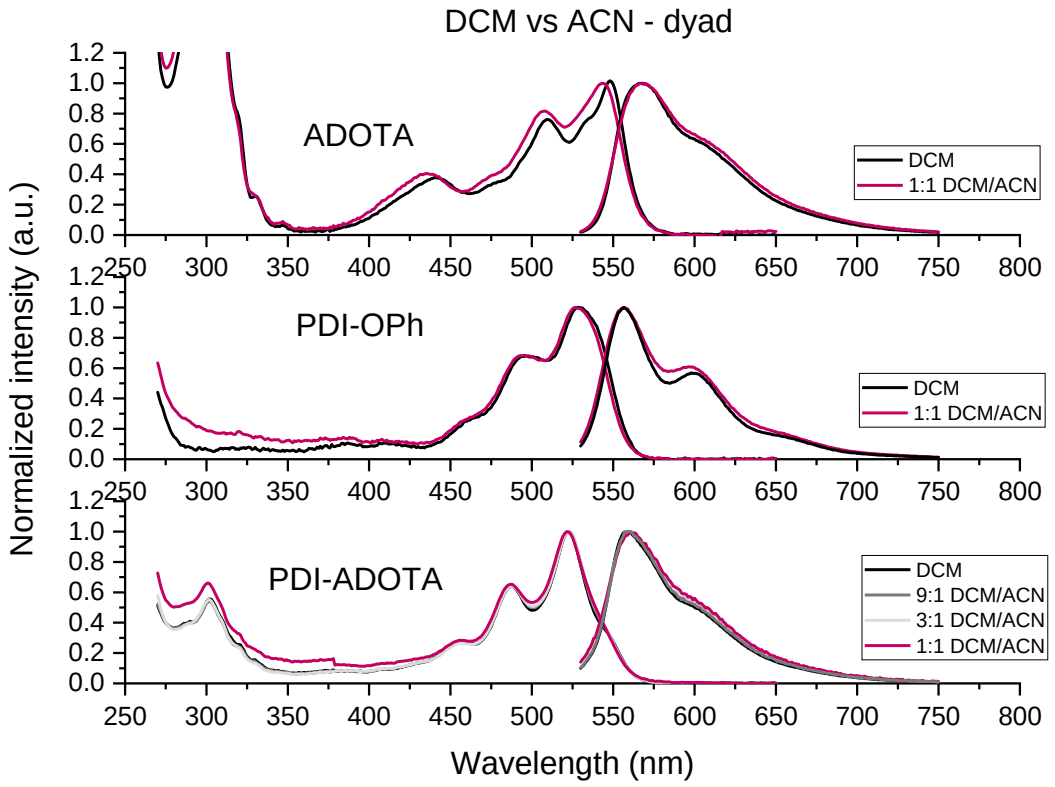

Figure S3. Normalized absorption and emission spectra in DCM and in DCM/ACN with 10, 25 and 50 v% ACN for ADOTA-PDI and 50 V% for the references.

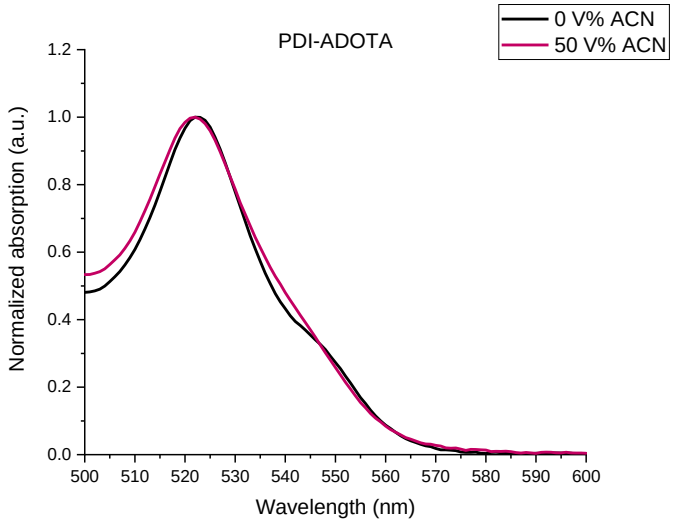

Figure S4. Zoom in of normalized absorption for PDI-ADOTA in DCM and in 50 v% ACN in DCM.

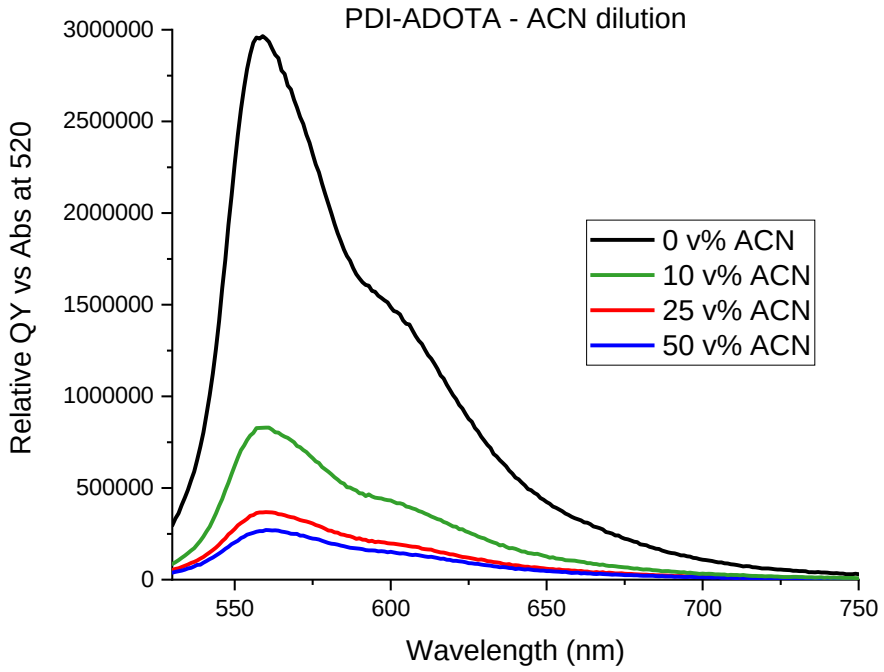

Figure S5. Relative emission quantum yield in 0, 10, 25 and 50 v% of ACN in DCM.

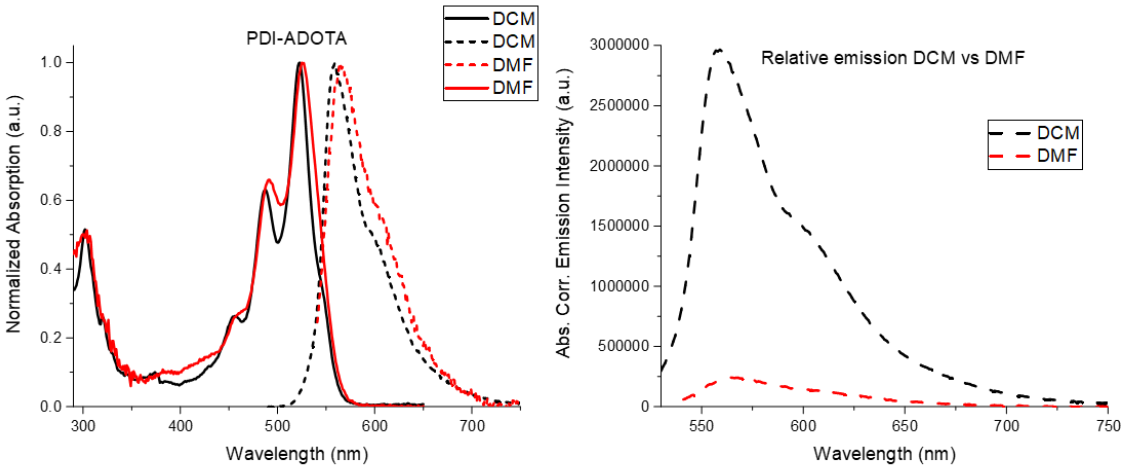

Figure S6. Right: Normalized absorption and emission of PDI-ADOTA in DCM and DMF. Left: Absorption corrected emission intensity.

Electrochemistry:

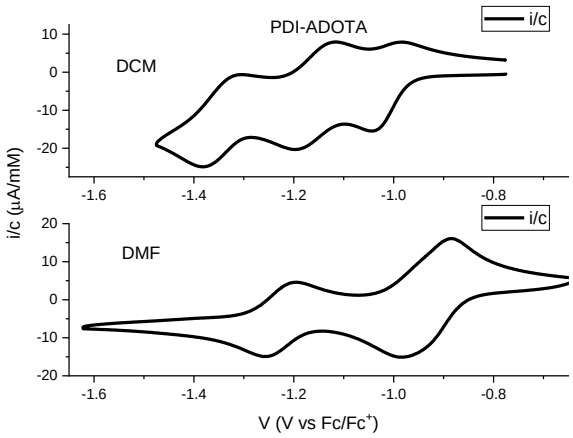

Figure S7. Cyclic Voltammograms of PDI-ADOTA in DCM and DMF.

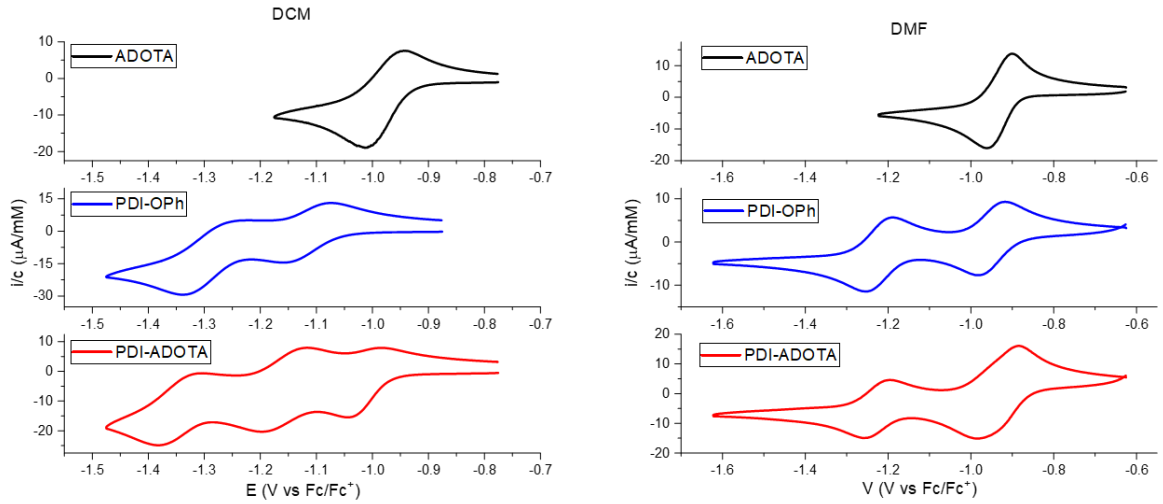

Figure S8. Cyclic voltammograms of ADOTA-Ref, PDI-OPh and PDI-ADOTA in DCM (left) and DMF (right).

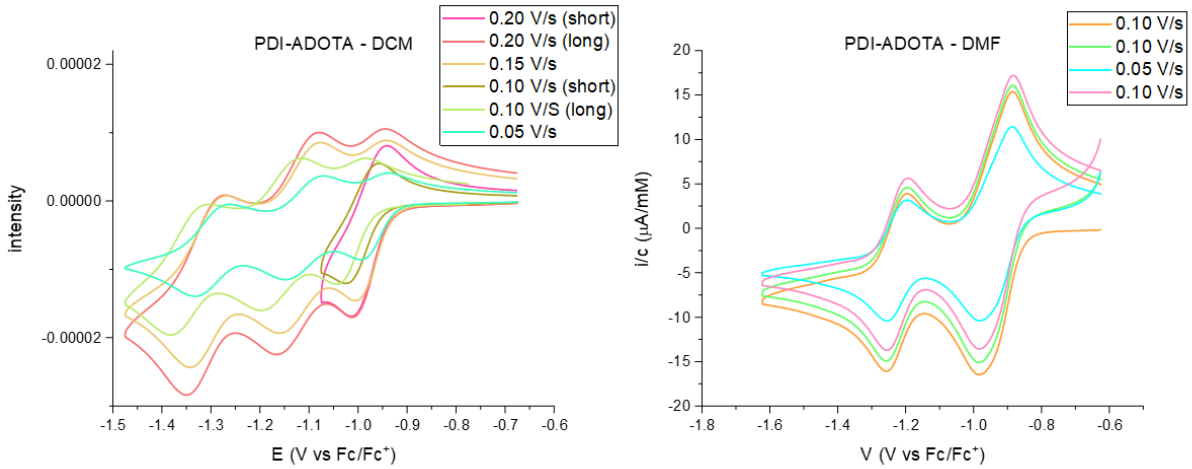

Figure S9. Cyclic voltammograms of PDI-ADOTA in DCM (left) and DMF (right) at multiple scan rates.

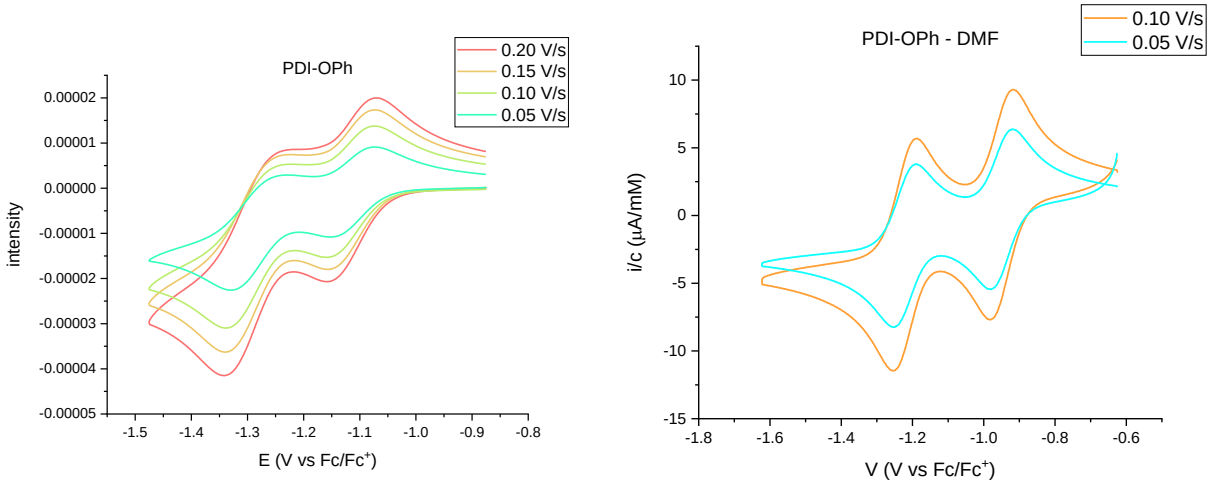

Figure S10. Cyclic voltammograms of PDI-OPh in DCM (left) and DMF (right) at multiple scan rates.

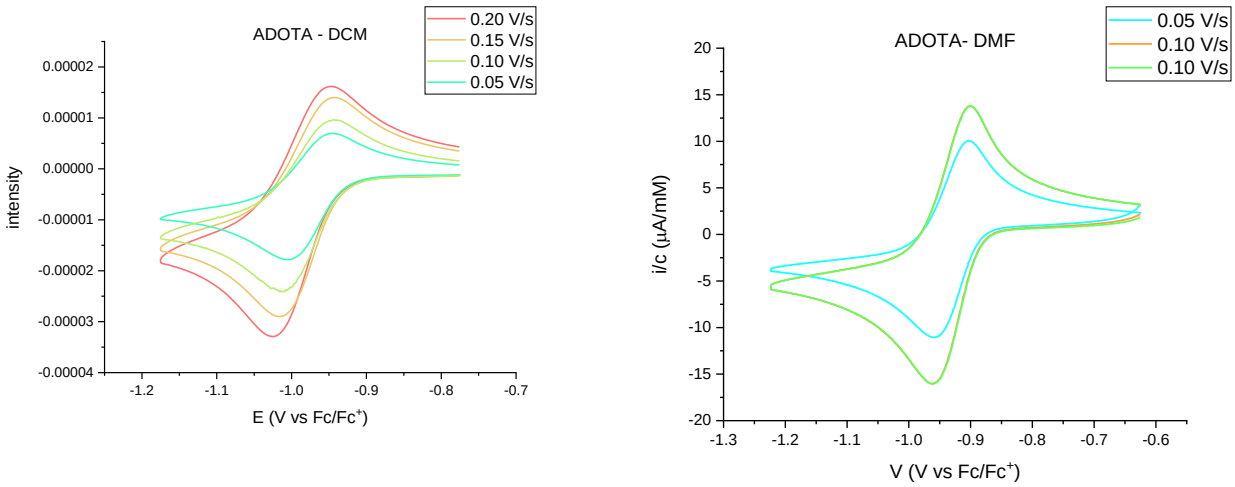

Figure S11. Cyclic voltammograms of ADOTA-Ref in DCM (left) and DMF (right) at multiple scan rates.

Transient absorption

Table S4. Lifetimes of local excited states found from global analysis of fs TA. The evolution associated spectra obtained from global analysis are shown in Figures S16.

	LE PDI	LE ADOTA Alone	PET-state and LE ADOTA
	τ_{PDI^*}	τ_{ADOTA^*}	$\tau_{ADOTA^*\text{-}PET}$
50 v% ACN in DCM	0.8 ± 0.2 ps	150 ± 10 ps	900 ± 200 ps
DCM	0.8 ± 0.2 ps	150 ± 10 ps	>>3000 ps

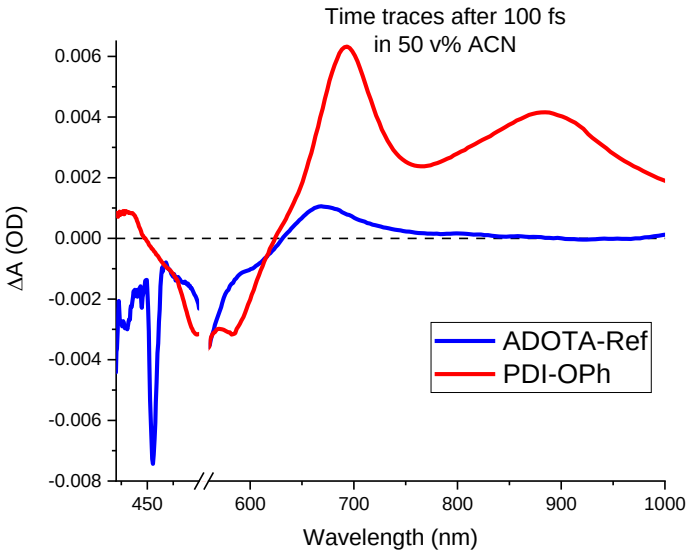

Figure S12. Overlay of Transient absorption spectra of PDI-OPh (Red) and ADOTA-Ref (blue) at decay time of ~100 fs, measured at similar concentrations and conditions.

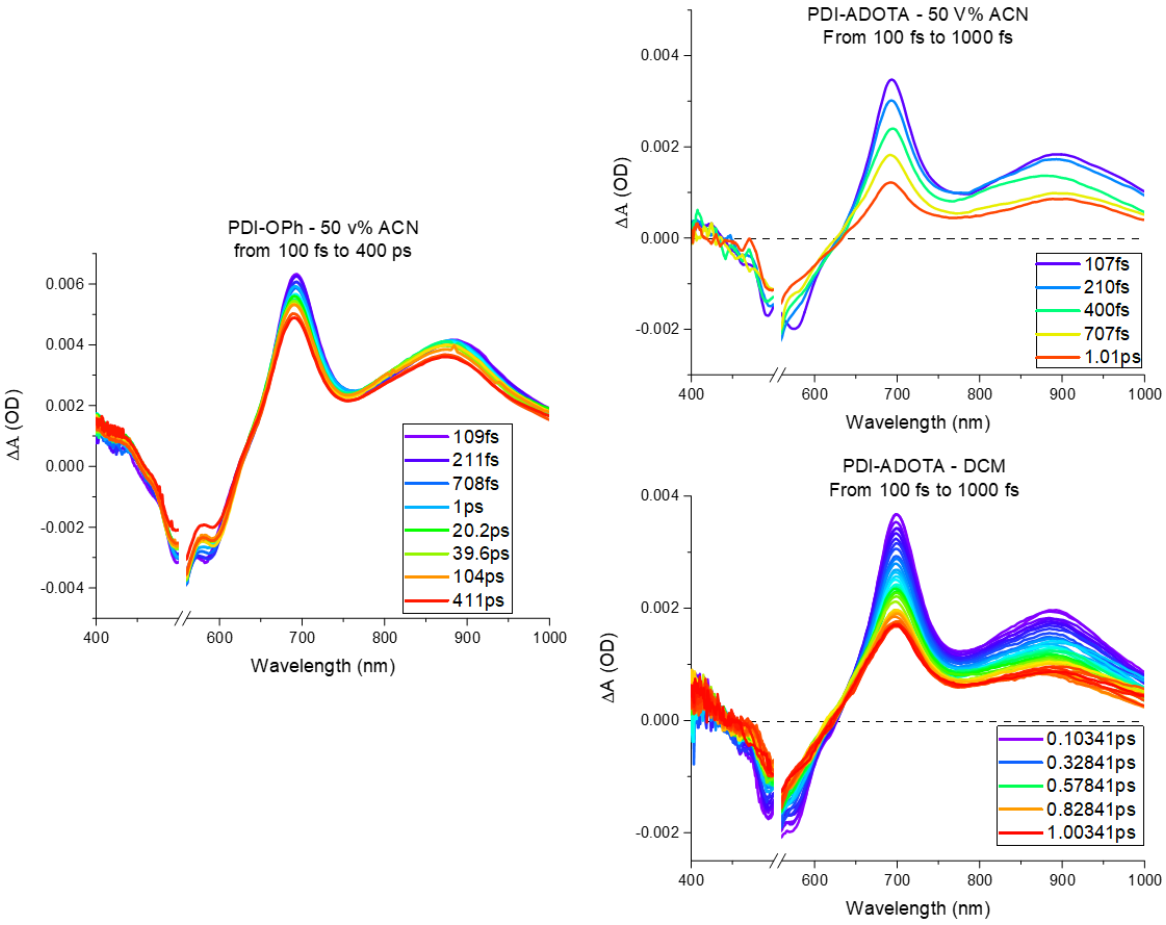

Figure S13. Spectral evolution fs-TA spectra over the time ranges of interest showing formation of LE-PDI in the dyad at early times. Left: PDI-OPh in 50 v% ACN, long lived excited-state of PDI. Right: PDI-ADOTA in 50 v% ACN and 0 v% ACN which matches the spectral features of PDI-OPh, proving the formation of LE PDI which decays much faster in the dyad (within 1 ps).

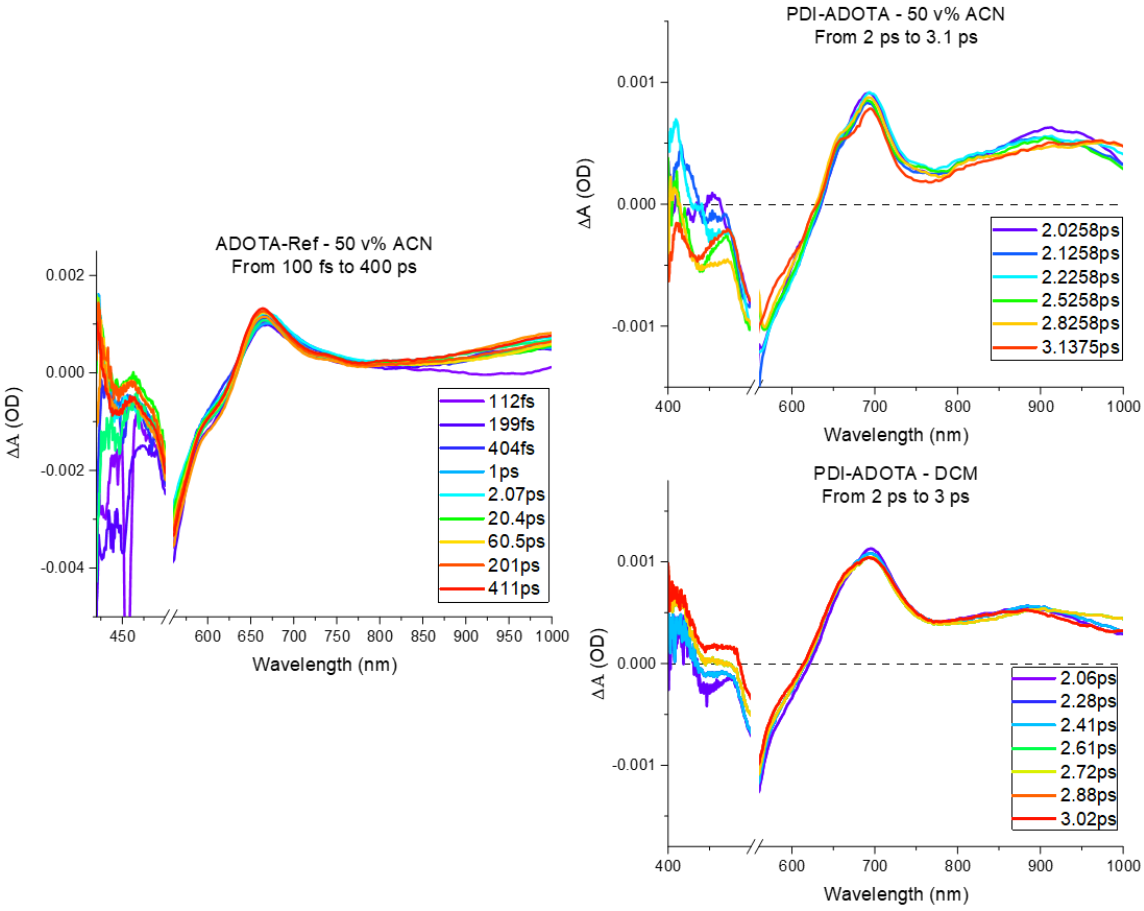

Figure S14. Spectral evolution fs-TA spectra over the time ranges of interest proving the formation of LE ADOTA. Left: ADOTA-Ref in 50 v% ACN showing the long lived excited ADOTA state. Right: PDI-ADOTA. Right: PDI-ADOTA in 50 v% ACN and 0 v% ACN matching with the spectral features of ADOTA-Ref, proving the formation of LE ADOTA in the dyad.

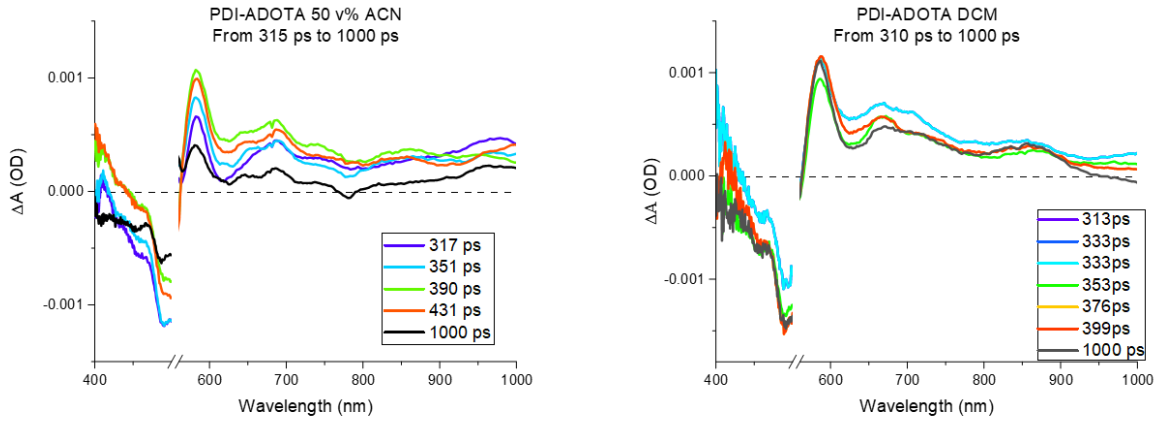

Figure S15. Spectral evolution fs-TA spectra over the time ranges of interest showing formation of the third state. Matching with the reported spectra of other oxidized perylene compunds proving the formation of thePET).

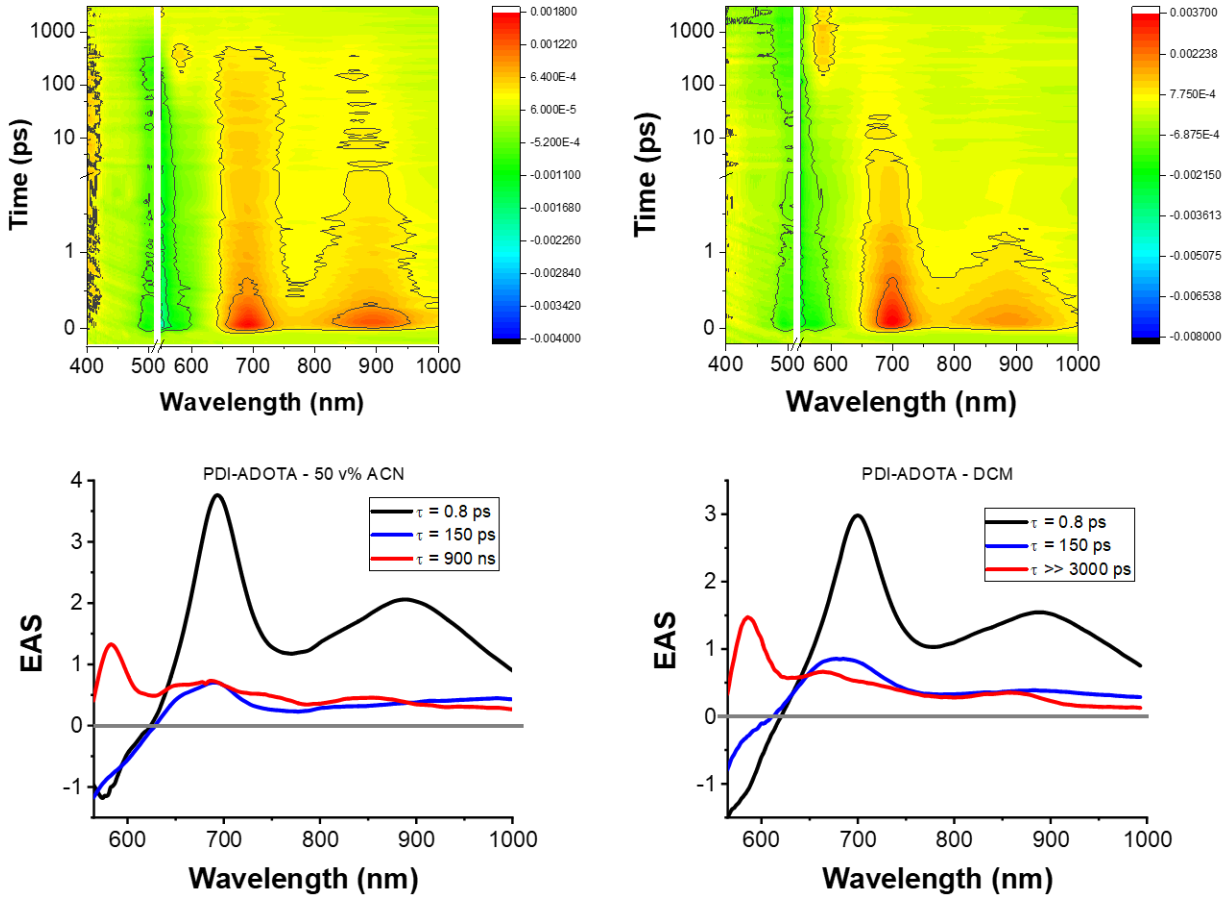

Figure S16. Top: Transient absorption spectra of PDI-ADOTA in 50 v% ACN and DCM. Bottom is evolution associated spectra (EAS) obtained from global analysis of the TA spectra with the lifetime of the three states reported in the legend.

Time Resolved Fluorescence Spectroscopy

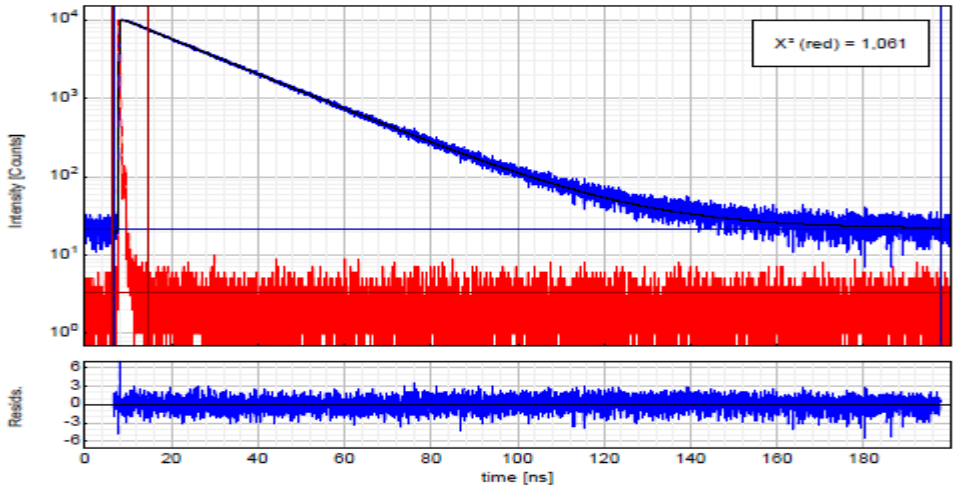

Parameter	Value	Conf. Lower	Conf. Upper	Conf. Estimation
A_1 [Cnts]	11992,7	-60,3	+60,3	Fitting
τ_1 [ns]	19,3557	-0,0728	+0,0728	Fitting
Bkgr. Dec [Cnts]	21,83	-1,28	+1,28	Fitting
Bkgr. IRF [Cnts]	3,39	-1,67	+1,67	Fitting
Shift IRF [ns]	0,02666	-0,00848	+0,00848	Fitting

Figure S17. ADOTA-Ref in DCM. Excited with 530 nm laser.

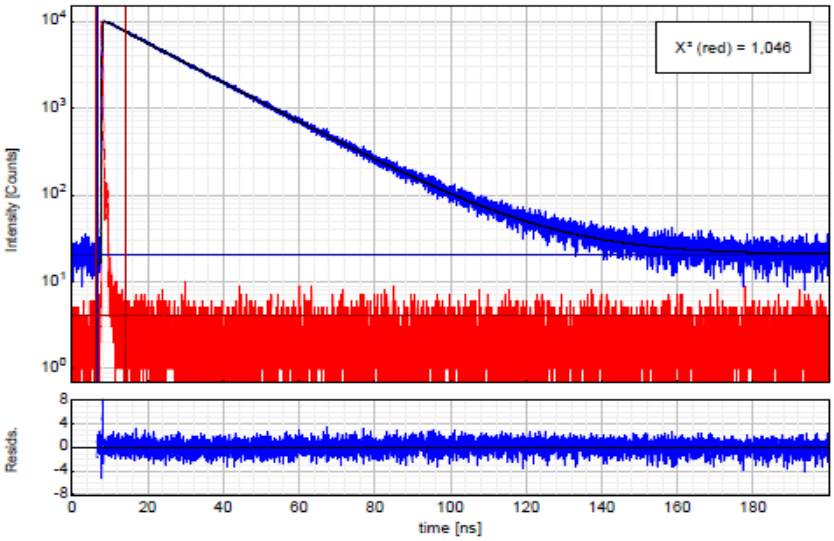

Parameter	Value	Conf. Lower	Conf. Upper	Conf. Estimation
A_1 [Cnts]	11965,2	-60,7	+60,7	Fitting
τ_1 [ns]	19,0401	-0,0718	+0,0718	Fitting
Bkgr. Dec [Cnts]	20,53	-1,21	+1,21	Fitting
Bkgr. IRF [Cnts]	4,03	-1,73	+1,73	Fitting
Shift IRF [ns]	-0,00291	-0,00775	+0,00775	Fitting

Figure S18. ADOTA-Ref in 50 v% in DCM. Excited with 530 nm laser.

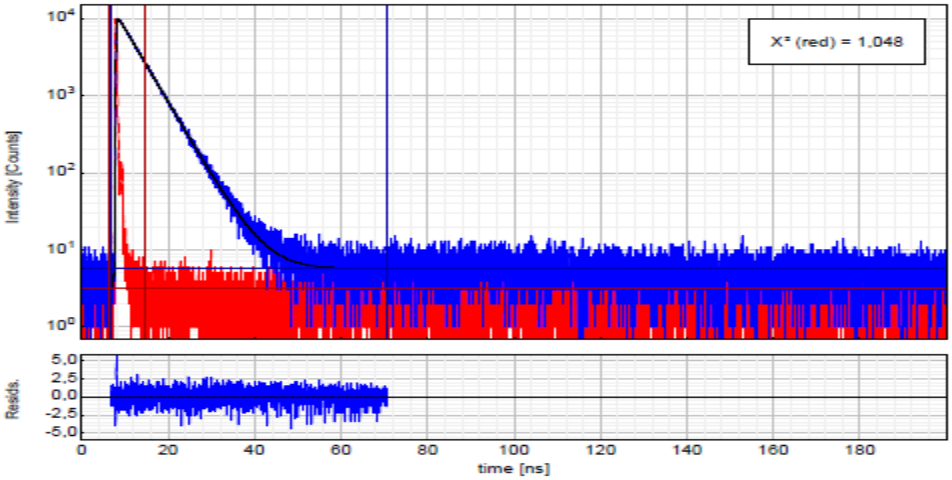

Parameter	Value	Conf. Lower	Conf. Upper	Conf. Estimation
A_1 [Cnts]	12894,0	-73,6	+73,6	Fitting
τ_1 [ns]	4,5628	-0,0189	+0,0189	Fitting
Bkgr. Dec [Cnts]	5,694	-0,640	+0,640	Fitting
Bkgr. IRF [Cnts]	3,22	-1,09	+1,09	Fitting
Shift IRF [ns]	0,03106	-0,00453	+0,00453	Fitting

Figure S19. PDI-OPh in DCM. Excited with 530 nm laser.

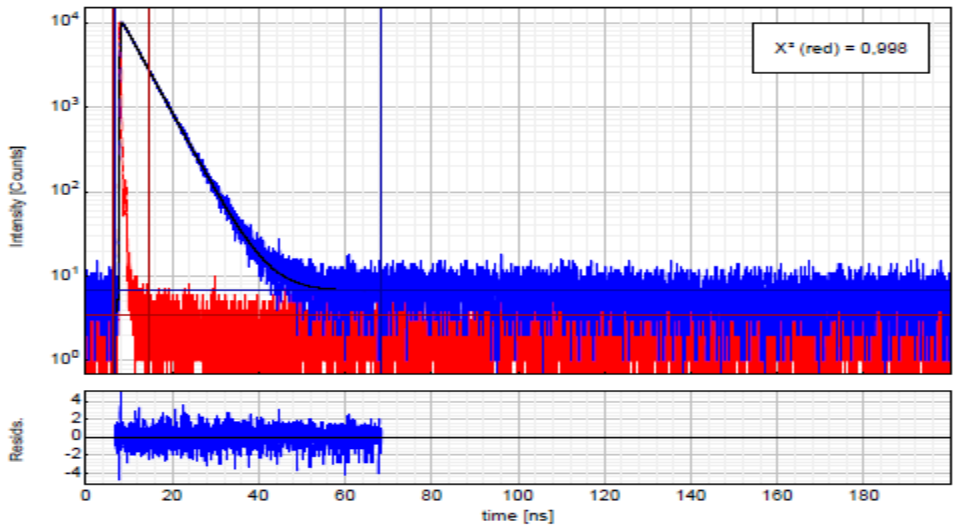

Parameter	Value	Conf. Lower	Conf. Upper	Conf. Estimation
A_1 [Cnts]	12955,2	-70,4	+70,4	Fitting
τ_1 [ns]	4,6372	-0,0183	+0,0183	Fitting
Bkgr. Dec [Cnts]	6,718	-0,680	+0,680	Fitting
Bkgr. IRF [Cnts]	3,400	-0,997	+0,997	Fitting
Shift IRF [ns]	0,00481	-0,00427	+0,00427	Fitting

Figure S20. PDI-OPh in 50 v% ACN in DCM. Excited with 530 nm laser.

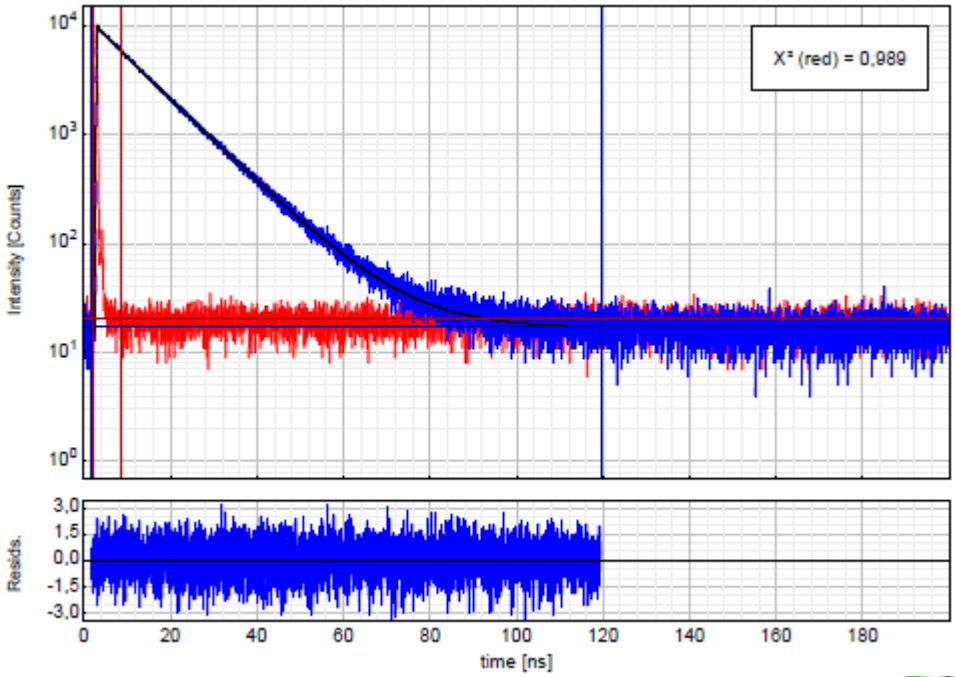

Parameter	Value	Conf. Lower	Conf. Upper	Conf. Estimation
A_1 [Cnts]	11530,5	-62,1	+62,1	Fitting
τ_1 [ns]	11,4050	-0,0446	+0,0446	Fitting
A_2 [Cnts]	601	-117	+117	Fitting
τ_2 [ns]	5,09	-1,07	+1,07	Fitting
A_3 [Cnts]	5514	-879	+879	Fitting
τ_3 [ns]	0,1964	-0,0376	+0,0376	Fitting
Bkgr. Dec [Cnts]	17,01	-1,08	+1,08	Fitting
Bkgr. IRF [Cnts]	20,26	-1,69	+1,69	Fitting
Shift IRF [ns]	0,01848	-0,00515	+0,00515	Fitting

Average Lifetime:

$\tau_{Av.1}$=11,1731 ns (intensity weighted)

$\tau_{Av.2}$=7,6874 ns (amplitude weighted)

Fractional Intensities of the Positive Decay Components:

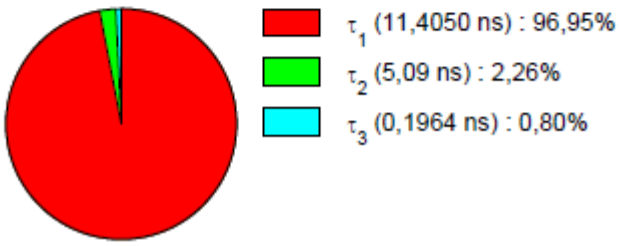

Figure S21. PDI-ADOTA in 0 v% ACN in DCM. Excited with 530 nm laser.

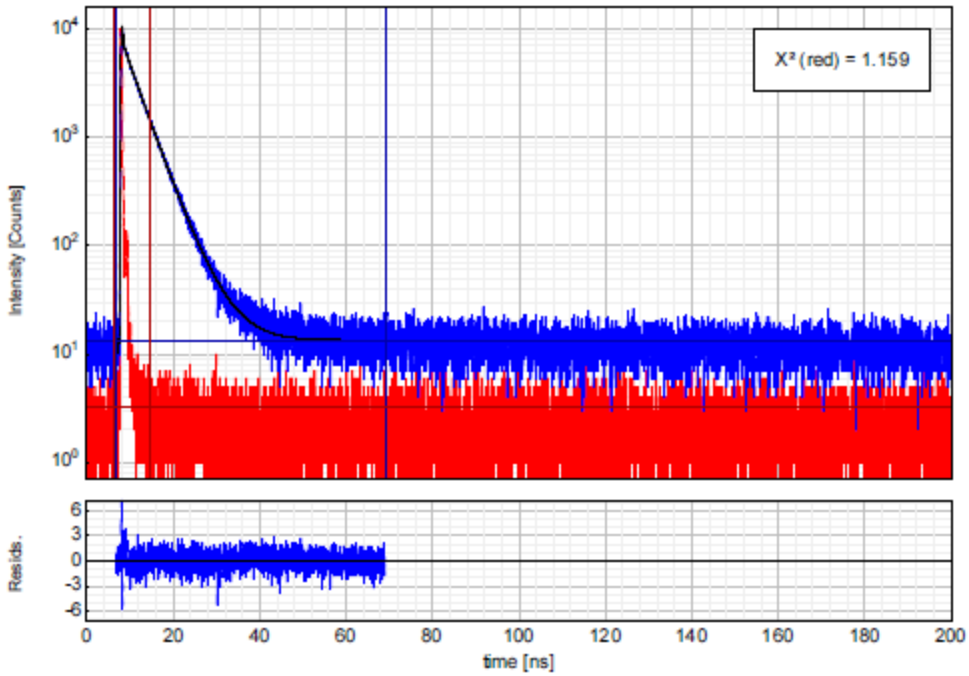

Parameter	Value	Conf. Lower	Conf. Upper	Conf. Estimation
A_1 [Cnts]	7030.7	-79.0	+79.0	Fitting
τ_1 [ns]	3.4860	-0.0306	+0.0306	Fitting
A_2 [Cnts]	2048.7	-52.4	+52.4	Fitting
τ_2 [ns]	5.100	---	---	<none>
A_3 [Cnts]	12919	-740	+740	Fitting
τ_3 [ns]	0.1835	-0.0113	+0.0113	Fitting
Bkgr. Dec [Cnts]	13.371	-0.876	+0.876	Fitting
Bkgr. IRF [Cnts]	3.27	-1.57	+1.57	Fitting
Shift IRF [ns]	0.03144	-0.00392	+0.00392	Fitting
A Scat [Cnts]	25330	-3440	+3440	Fitting

Average Lifetime:

$\tau_{Av.1}$=3.7280 ns (intensity weighted)

$\tau_{Av.2}$=1.6969 ns (amplitude weighted)

Fractional Intensities of the Positive Decay Components:

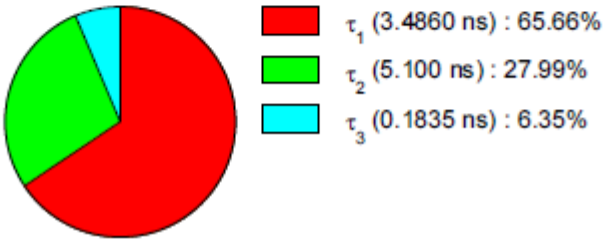

Figure S22. PDI-ADOTA in 10 v% ACN in DCM. Excited with 530 nm laser. 5.1 ns locked to match with the other FLTs.

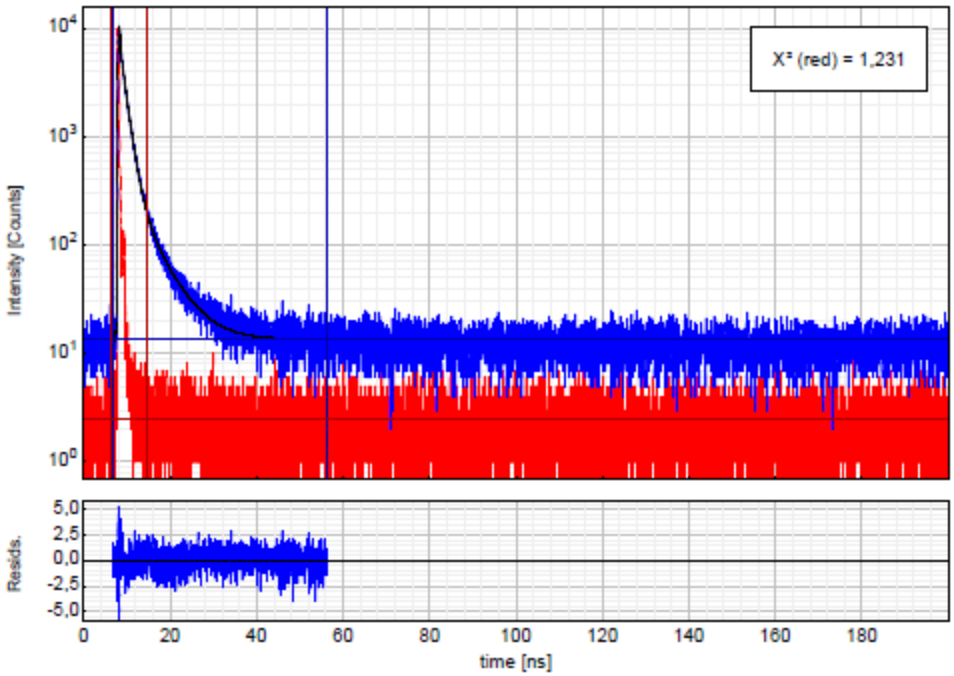

Parameter	Value	Conf. Lower	Conf. Upper	Conf. Estimation
A_1 [Cnts]	547,3	-23,0	+23,0	Fitting
τ_1 [ns]	5,086	-0,126	+0,126	Fitting
A_2 [Cnts]	9343	-130	+130	Fitting
τ_2 [ns]	1,3107	-0,0142	+0,0142	Fitting
A_3 [Cnts]	15260	-617	+617	Fitting
τ_3 [ns]	0,20117	-0,00872	+0,00872	Fitting
Bkgr. Dec [Cnts]	13,480	-0,868	+0,868	Fitting
Bkgr. IRF [Cnts]	2,50	-1,51	+1,51	Fitting
Shift IRF [ns]	0,03006	-0,00364	+0,00364	Fitting

Average Lifetime:

$\tau_{Av.1}$=1,703 ns (intensity weighted)

$\tau_{Av.2}$=0,720 ns (amplitude weighted)

Fractional Intensities of the Positive Decay Components:

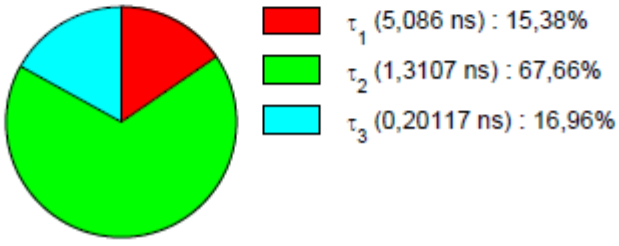

Figure S23. PDI-ADOTA in 25 v% ACN in DCM. Excited with 530 nm laser.

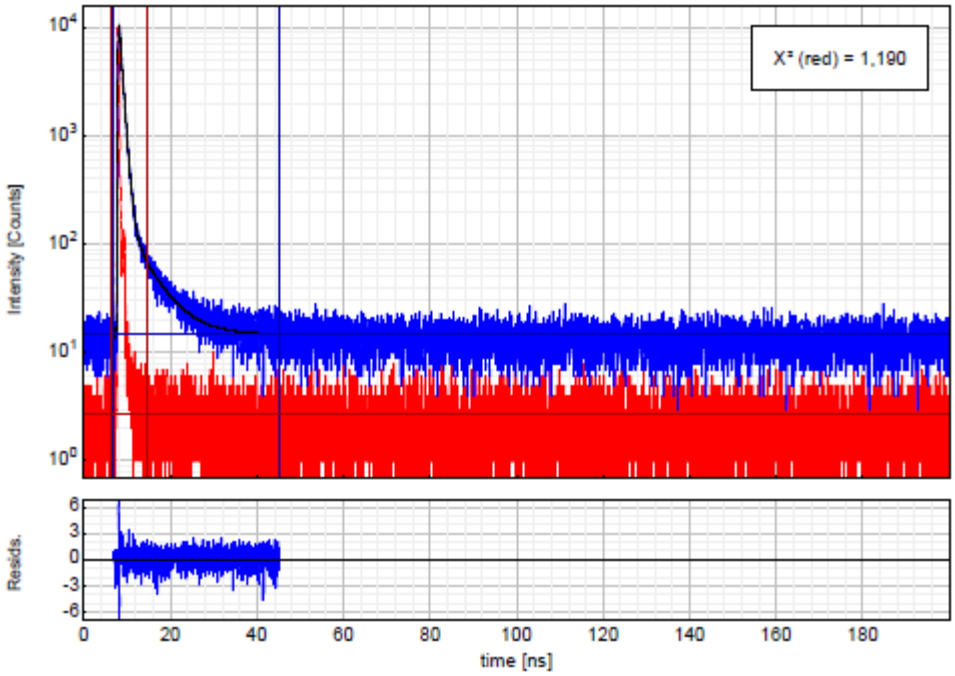

Parameter	Value	Conf. Lower	Conf. Upper	Conf. Estimation
A_1 [Cnts]	212,9	-12,0	+12,0	Fitting
τ_1 [ns]	5,196	-0,200	+0,200	Fitting
A_2 [Cnts]	15496	-187	+187	Fitting
τ_2 [ns]	0,68124	-0,00629	+0,00629	Fitting
A_3 [Cnts]	21240	-1330	+1330	Fitting
τ_3 [ns]	0,07372	-0,00441	+0,00441	Fitting
Bkgr. $_{Dec}$ [Cnts]	14,804	-0,881	+0,881	Fitting
Bkgr. $_{IRF}$ [Cnts]	2,74	-1,25	+1,25	Fitting
Shift $_{IRF}$ [ns]	0,01915	-0,00271	+0,00271	Fitting

Average Lifetime:

$\tau_{Av.1}$=0,987 ns (intensity weighted)

$\tau_{Av.2}$=0,358 ns (amplitude weighted)

Fractional Intensities of the Positive Decay Components:

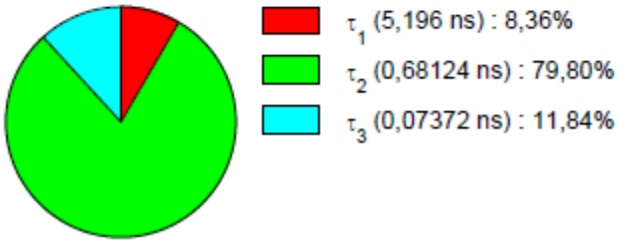

Figure S24. PDI-ADOTA in 50 v% ACN in DCM. Excited with 530 nm laser.

Chemical reduction data:

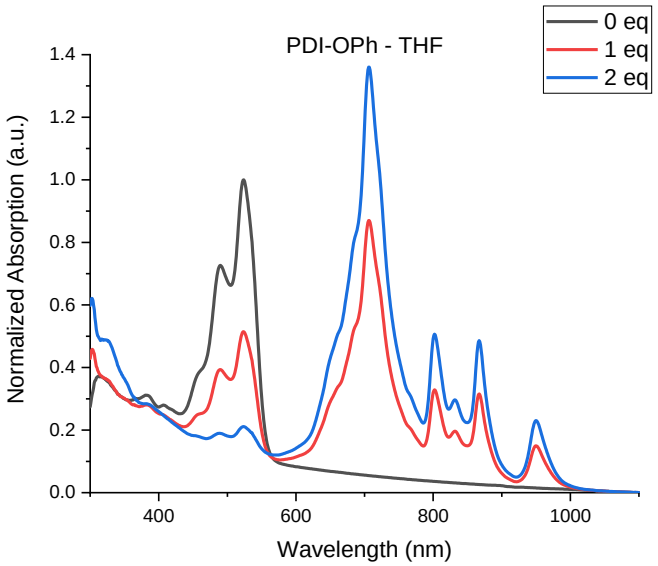

Figure S25. Relative absorption of PDI-OPh in THF with 0-2 equivalents of $CoCp_2$.

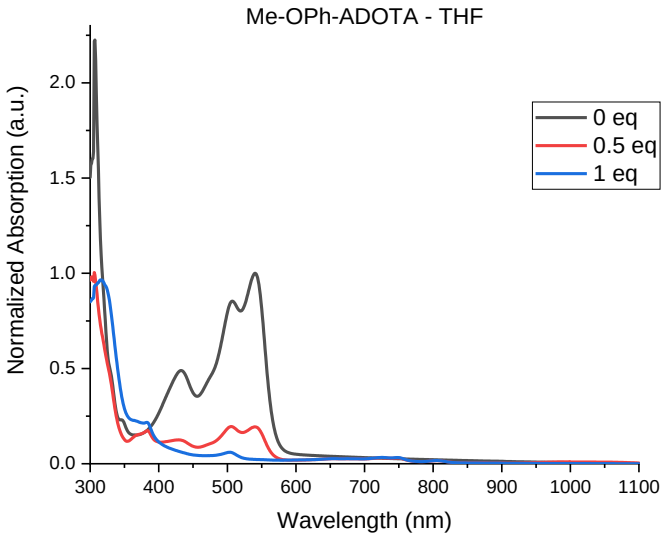

Figure S26. Relative absorption of ADOTA-Ref in THF with 0-1 equivalents of $CoCp_2$.

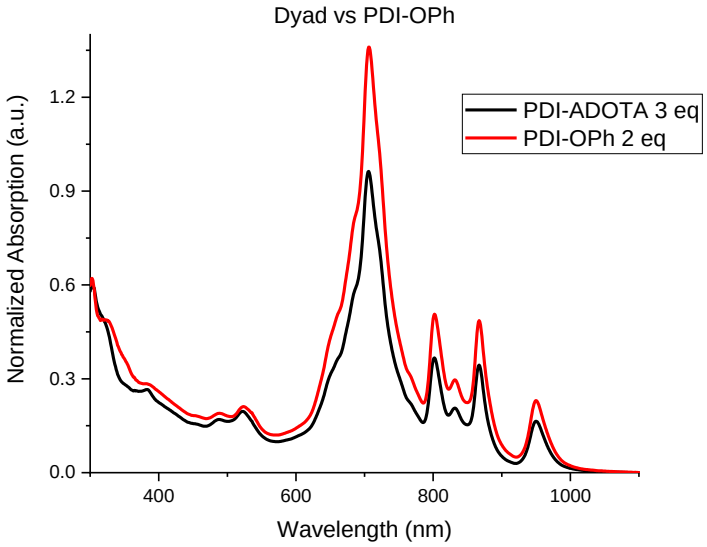

Figure S27. Overlay of relative absorption in THF of PDI-OPh with 2 equivalents $CoCp_2$ and PDI-ADOTA with 3 equivalents of $CoCp_2$.

NMR spectra:

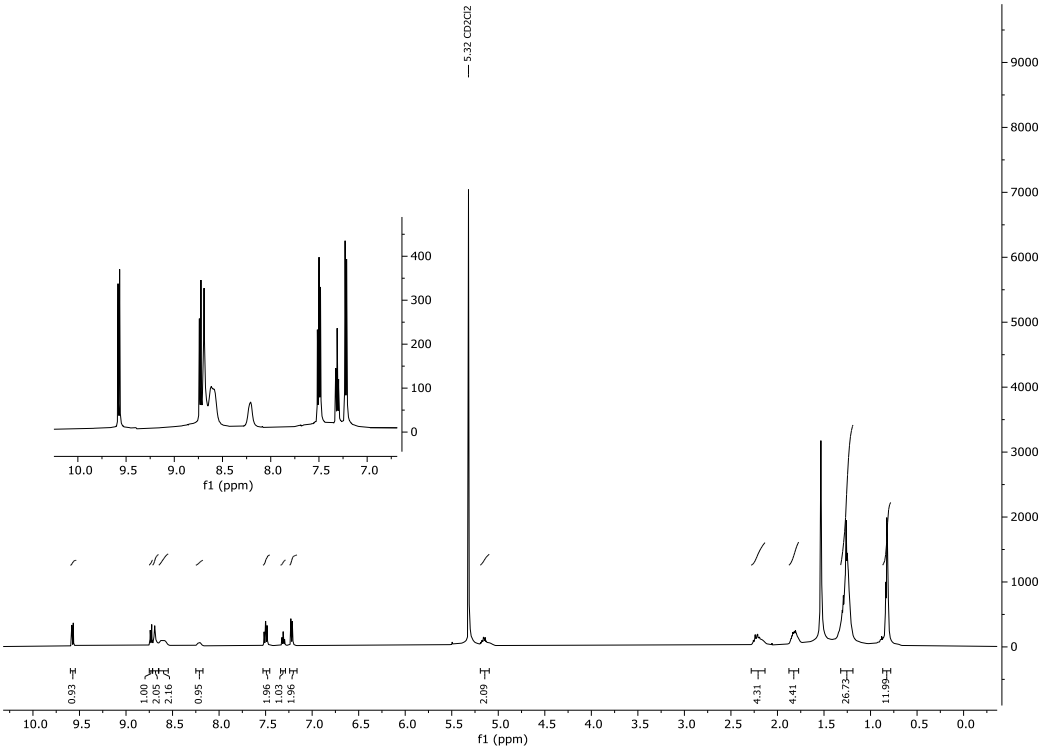

Figure S28 ^{1}H-NMR of PDI-OPh in CD_2Cl_2.

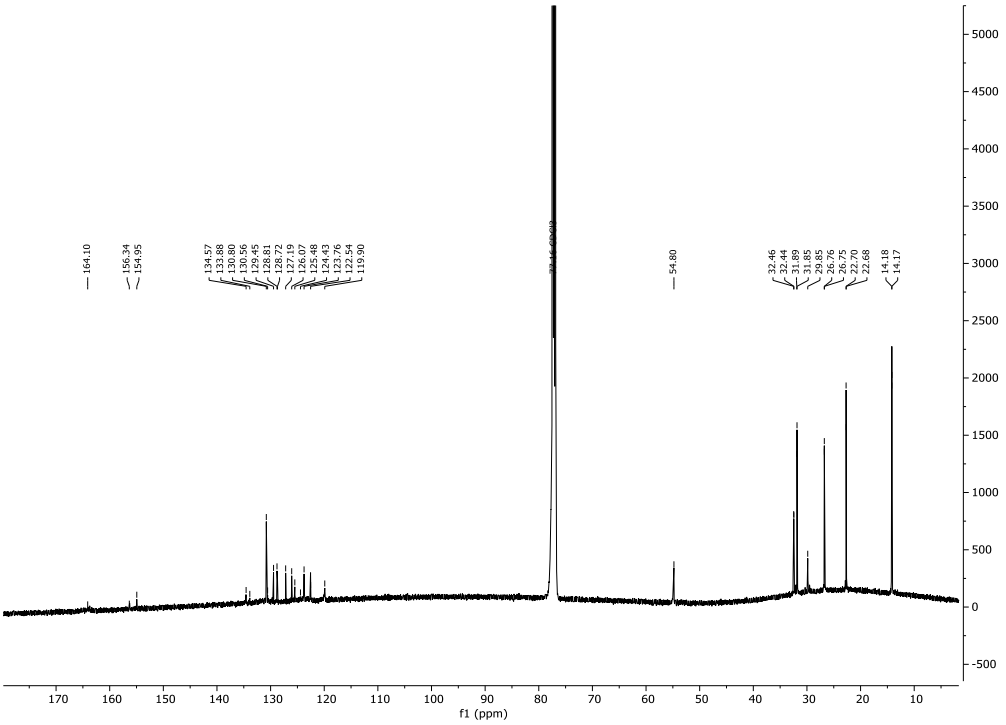

Figure S29 ^{13}C-NMR of PDI-OPh in $CDCl_3$. Some of the quatenary carbon signals are not identifiable due to overlapping signals, and in general broad signal e.g. like the imide carbon at ~164 ppm. This is due to

changes occuring in the conformation hence longer delay time and increasing number of scans is not going to increase the resolution. Similar results have been reported forother mono bay substitutied PDIs.[7]

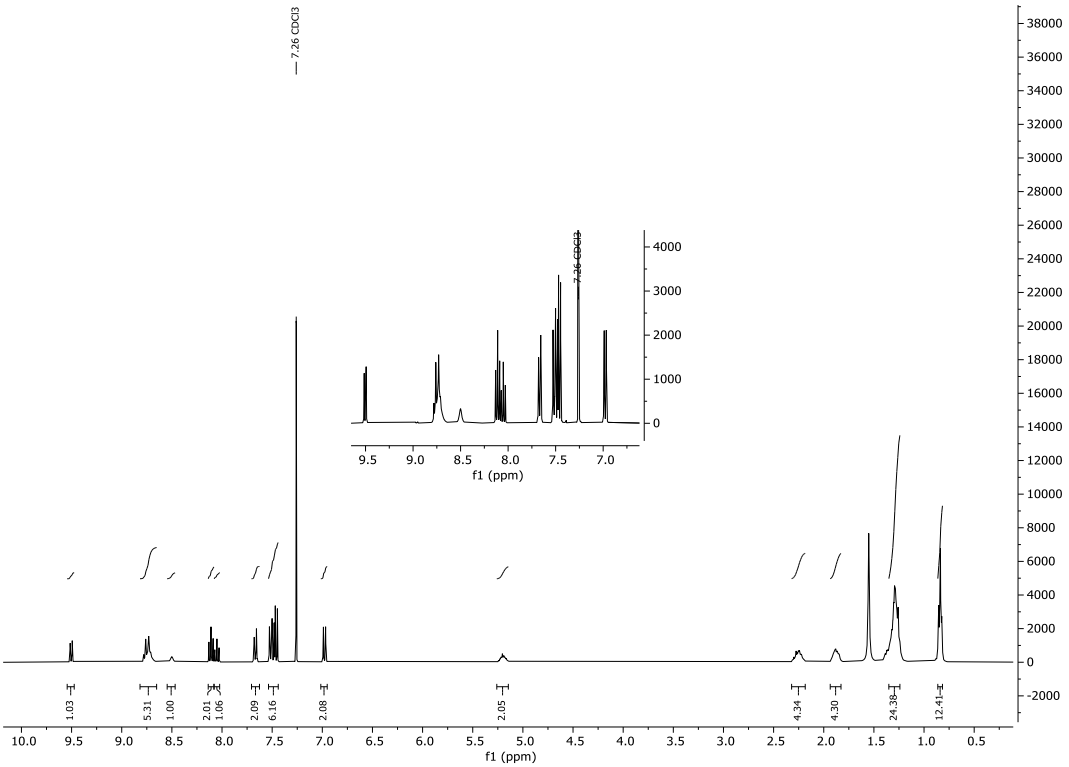

Figure S30. ^{1}H-NMR of PDI-ADOTA in $CDCl_3$.

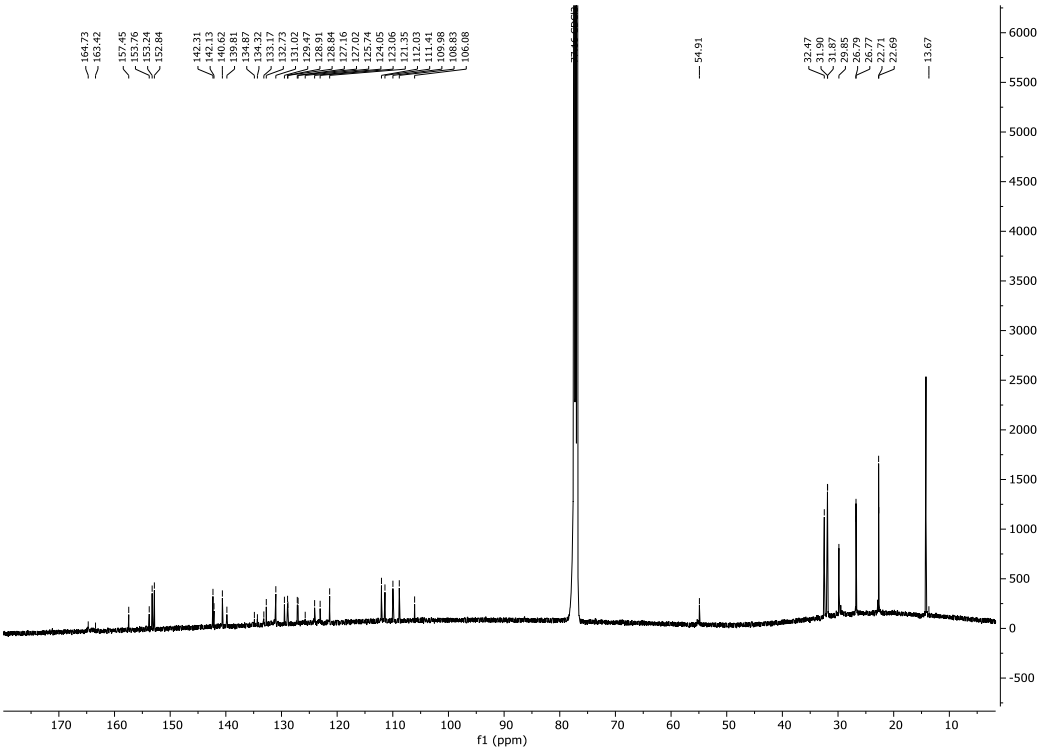

Figure S31. ^{13}C-NMR of PDI-ADOTA in $CDCl_3$. Some of the quatenary carbon signals are not identifiable due to overlapping signals, and in general broad signal e.g. like the imide carbon at 164 ppm. This is due to changes occuring in the conformation hence longer delay time and increasing number of scans is not going to increase the resolution. Similar results have been reported forother mono bay substitutied PDIs.[7]

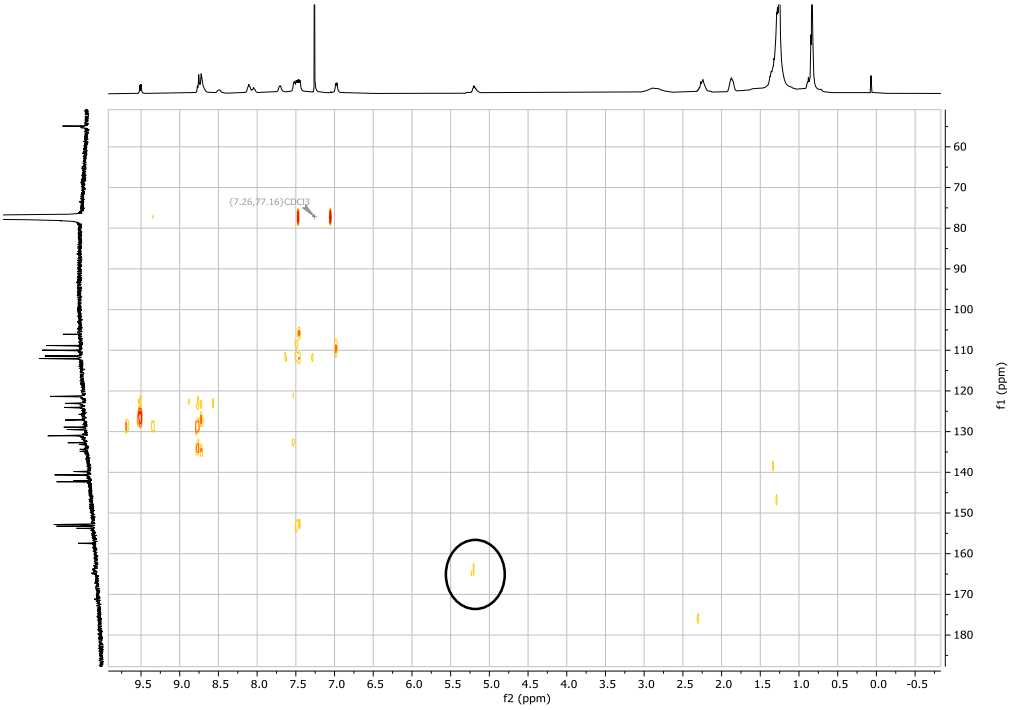

Figure S32. HMBC spectra of PDI-ADOTA in $CDCl_3$. Weak imide carbon signals highlighted with a black cirle in the HMBC.

References:

(1) Rajasingh, P.; Cohen, R.; Shirman, E.; Shimon, L. J. W.; Rybtchinski, B. Selective Bromination of Perylene Diimides under Mild Conditions. *The Journal of Organic Chemistry* **2007**, *72* (16), 5973-5979. DOI: 10.1021/jo070367n.
(2) Rosenberg, M.; Junker, A. K. R.; Sørensen, T. J.; Laursen, B. W. Fluorescence pH Probes Based on Photoinduced Electron Transfer Quenching of Long Fluorescence Lifetime Triangulenium Dyes. *Chemphotochem* **2019**, *3* (5), 233-242. DOI: 10.1002/cptc.201800266.
(3) Lin, M.-J.; Jiménez, Á. J.; Burschka, C.; Würthner, F. Bay-substituted perylene bisimide dye with an undistorted planar scaffold and outstanding solid state fluorescence properties. *Chemical Communications* **2012**, *48* (99), 12050. DOI: 10.1039/c2cc36719j.
(4) Bogh, S. A.; Simmermacher, M.; Westberg, M.; Bregnhoj, M.; Rosenberg, M.; De Vico, L.; Veiga, M.; Laursen, B. W.; Ogilby, P. R.; Sauer, S. P. A.; et al. Azadioxatriangulenium and Diazaoxatriangulenium: Quantum Yields and Fundamental Photophysical Properties. *Acs Omega* **2017**, *2* (1), 193-203. DOI: 10.1021/acsomega.6b00211.
(5) Snellenburg, J. J.; Laptenok, S.; Seger, R.; Mullen, K. M.; van Stokkum, I. H. M. Glotaran: A Java-Based Graphical User Interface for the R Package TIMP. *Journal of Statistical Software* **2012**, *49* (3), 1 - 22. DOI: 10.18637/jss.v049.i03 (acccessed 2023/03/22).
(6) van Stokkum, I. H. M.; Larsen, D. S.; van Grondelle, R. Global and target analysis of time-resolved spectra. *Bba-Bioenergetics* **2004**, *1657* (2-3), 82-104. DOI: DOI 10.1016/j.bbabio.2004.04.011.
(7) Zhang, F.; Zhang, Z.; Deng, L.; Guo, H.; Xia, T.; Mao, W.; Zhang, J. Green-Light Responsive Perylene Bisimides for Atom-Economic Thiol Generation and Click-Ligation. *Organic Letters* **2023**, *25* (5), 872-876. DOI: 10.1021/acs.orglett.3c00101.